Joint Molecular Modeling and Spectroscopic Studies of DNA Complexes of a Bis(arginyl) Conjugate of a Tricationic Porphyrin Designed to Target the Major Groove†

Shahla Mohammadi,‡ Martine Perrée-Fauvet,*,§ Nohad Gresh,|| Karine Hillairet,§ and Eliane Taillandier‡

Laboratoire de Chimie Structurale et Spectroscopie Biomoléculaire (CNRS-URA 1430), Université Paris 13, F-93017 Bobigny Cedex, France; Laboratoire de Chimie Bioorganique et Bioinorganique (CNRS-URA 1384), Université Paris 11, F-91405 Orsay Cedex, France; and Laboratoire de Pharmacochimie Moléculaire et Structurale (CNRS-URA 1500, INSERM U266), Université Paris 5, F-75270 Paris Cedex 06, France

Received December 3, 1997; Revised Manuscript Received March 2, 1998

ABSTRACT: To target selectively the major groove of double-stranded B DNA, we have designed and synthesized a bis(arginyl) conjugate of a tricationic porphyrin (BAP). Its binding energies with a series of double-stranded dodecanucleotides, having in common a central $d(CpG)_2$ intercalation site were compared. The theoretical results indicated a significant energy preference favoring major groove over minor groove binding and a preferential binding to a sequence encompassing the palindrome GGCGCC encountered in the Primary Binding Site of the HIV-1 retrovirus. Spectroscopic studies were carried out on the complexes of BAP with poly(dG-dC) and poly(dA-dT) and a series of oligonucleotide duplexes having either a GGCGCC, CCCGGG, or TACGTA sequence. The results of UV−visible and circular dichroism spectroscopies indicated that intercalation of the porphyrin takes place in poly(dG-dC) and all the oligonucleotides. Thermal denaturation studies showed that BAP increased significantly the melting temperature of the oligonucleotides having the GGCGCC sequence, whereas it produced only a negligible stabilization of sequences having CCCGGG or TACGTA in place of GGCGCC. This indicates a preferential binding of BAP to GGCGCC, fully consistent with the theoretical predictions. IR spectroscopy on $d(GGCGCC)_2$ indicated that the guanine absorption bands, $C_6{=}O_6$ and $N_7{-}C_8{-}H$, were shifted by the binding of BAP, indicative of the interactions of the arginine arms in the major groove. Thus, the *de novo* designed compound BAP constitutes one of the very rare intercalators which, similar to the antitumor drugs mitoxantrone and ditercalinium, binds DNA in the major groove rather than in the minor groove.

The palindromic $d(GGCGCC)_2$ sequence, frequently encountered in oncogenes *(1*−*5*), is also a mutational hot spot in DNA *(6*), and the recognition sequence of the *Nar*I restriction enzyme *(7*). It is part of the Primary Binding Site of the Long Terminal Repeat of the HIV-1 retrovirus *(8, 9*), thus a most important target for the design of novel drugs that would selectively recognize and bind it. For that purpose, we have recently designed and synthesized a bis(arginyl) derivative of a tricationic porphyrin (BAP) *(10*), whose molecular structure is represented in Figure 1.

The rationale for the design of BAP was grounded on the following two essential considerations:

(1) Choice of the Porphyrin. The bis(arginyl)porphyrin BAP is a derivative of the tetracationic *meso*-tetrakis(*N*-methyl-4-pyridiniumyl)porphyrin (H_2TMPyP-4) which is able to bind strongly to GC-rich sequences by intercalation *(11*−*13*). Since among the GC-rich dinucleotides the pyrimidine−purine dinucleotide $d(CpG)_2$ is the most favored energy-wise for intercalation *(14*−*17*), the strong affinity of cationic intercalating porphyrins for DNA should anchor the drug in the center of the targeted $d(GGCGCC)_2$ hexamer at the $d(CpG)_2$ site. If extending its recognition sequence from two to six base-pairs with the help of arginine arms could be achieved, it should obviously be more efficient and specific for binding.

The tetracationic *meso*-tetrakis(*N*-methyl-4-pyridiniumyl)-porphyrin is endowed with strong antitumor activities *(18*), while eliciting weak toxic effects *(19*). Furthermore, cationic porphyrins and metalloporphyrins were shown to display nuclease activities *(20*−*25*).

(2) Selection of Arginine as Recognition Units. Our present goal is to target guanine bases which are upstream from the intercalation site on both strands. The selection of arginine is grounded on the original proposals of Seeman et al. *(26*) and Hélène *(27*). Recent papers reported that this amino acid shows the strongest preferential binding to guanine in the major groove, compared to the other bases *(28*−*35*). Numerous examples exist, from both high-resolution X-ray *(36*−*39*) and NMR spectroscopy *(40*) of

†This work was supported by the Agence Nationale de Recherche sur le Sida (ANRS) which is personally acknowledged by one of us (K.H.) for financial support.

* To whom correspondence should be addressed. E-mail: mperreef@icmo.u-psud.fr; Fax: 33 1 69 15 72 81.

‡ Laboratoire de Chimie Structurale et Spectroscopie Biomoléculaire.

§ Laboratoire de Chimie Bioorganique et Bioinorganique.

|| Laboratoire de Pharmacochimie Moléculaire et Structurale.

S0006-2960(97)02964-4 CCC: $15.00
Published on Web 04/11/1998

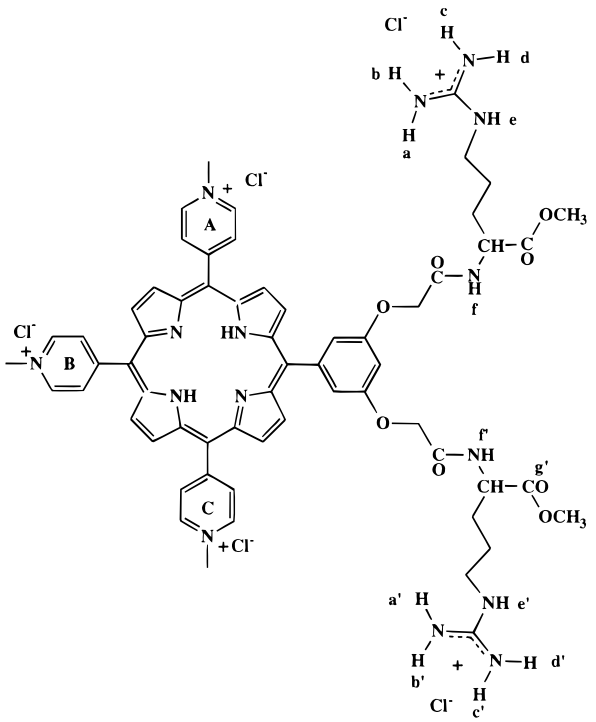

FIGURE 1: The bis(arginyl) derivative of the tricationic porphyrin (BAP). Molecular structure.

bidentate guanine−arginine interactions, involving O_6/N_7 of guanine and the guanidinium protons of arginine. The symmetrical disposition of the two peptide arms with respect to the chromophore is a reflection of the palindromic nature of the targeted sequence.

The present study is part of our current endeavors for the *de novo* design of oligopeptide intercalator molecules targeting well-defined DNA sequences in the *major* groove, as was illustrated in previous papers from our laboratories *(10, 41−44)*. To our knowledge, the sole efforts in this field relate to metallointercalator conjugates, such as 13-mer oligopeptides coupled to rhodium phenanthroline *(45)*. Other intercalator *(46, 47, and refs therein)*, metallointercalator−oligopeptide conjugates *(48)* as well as covalently bound oligopeptides *(49)*, resorted to peptide sequences which are the same as those of naturally occurring transcriptional activators. Instead of peptide side-chains, the earliest efforts to target the major groove used the nucleic acid bases themselves, molecular recognition of the complementary strand occurring through Watson−Crick or Hoogsteen base-pairing. These bases can be borne by either a natural or a modified sugar−phosphate backbone, as with antisense RNA or triple-helix forming DNA conjugates *(50−54)*, by an oligopeptide *(55)*, or by a polycation ribonucleic guanidine backbone *(56)*. In contrast, most antitumor drugs, whether intercalating *(57, 58)* or nonintercalating *(59, 60)*, bind DNA in the *minor* groove. This is also the case for *virtually all* synthetic sequence-specific oligopeptides, whether nonintercalating *(61−64)* or covalently bound to an intercalator *(65−70)*. Yet the minor groove has, with respect to the major groove, a much more reduced potentiality for selective recognition, since its two principal electron-rich sites, N_3 of adenine and O_2 of thymine, not only occupy very similar positions in the B-DNA conformation, but have similar affinities for an incoming ligand as well, making them virtually indistinguishable *(71)*.

In an attempt to verify experimentally the models proposed by molecular modeling, a series of complexes of BAP with different DNAs has been studied by UV−visible, circular dichroism (CD), and FTIR spectroscopies. The investigated DNAs are sperm salmon DNA, poly(dG-dC), poly(dA-dT), or oligonucleotides having either a GGCGCC, CCCGGG, or TACGAT sequence. Visible absorption spectroscopy and circular dichroism are useful methods to demonstrate the mode of association of porphyrins with DNA *(72)*. UV thermal denaturation measurements give reliable data to evaluate the stabilization of the duplexes upon complexation, thus reflecting the binding affinity of the ligand. FTIR spectroscopy is used to detect the interaction sites in the major or minor groove of DNA duplexes.

We report in this paper the results of our joint molecular modeling and spectroscopic investigation.

MATERIALS AND METHODS

Materials. The bis(arginyl) derivative of the tricationic porphyrin BAP and the *meso*-tetrakis(*N*-methyl-4-pyridiniumyl)porphyrin (H_2TMPyP-4) were synthesized according to previously published procedures *(10, 73)*. The porphyrin concentrations were determined from visible absorption at the Soret maximum band by using $\epsilon_{424} = 2.17 \times 10^5$ M^{-1} cm^{-1} for BAP *(10)* and $\epsilon_{421} = 2.26 \times 10^5$ $M^{-1}cm^{-1}$ for H_2TMPyP-4 *(73)*.

The oligonucleotides used in the spectrosopic measurements were as follows: d(GTGGCGCCCGAA)·d(TTCGGGCGCCAC), $d(ATTACGTAAT)_2$, $d(GTGGCGCCAC)_2$, $d(GTCCCGGGAC)_2$, $d(GTTACGTAAC)_2$, $d(GGCGCC)_2$, $d(CCCGGG)_2$, $d(TACGTA)_2$.

They were purchased from Eurogentec, and purified and desalted using an Ultra-MC filter (Millipore). Their concentrations were determined by measuring their maximum absorption at 260 nm (25 °C) using an extinction coefficient (ϵ_{260}) calculated according to a closest neighbor model *(74)*. The ϵ_{260} (M^{-1} cm^{-1}/base) used for the oligonucleotides were as follows: d(GTGGCGCCCGAA) = 9491; d(TTCGGGCGCCAC) = 8725; d(ATTACGTAAT) = 10460; d(GTGGCGCCAC) = 9000; d(GTCCCGGGAC) = 9220; d(GTTACGTAAC) = 10020; d(GGCGCC) = 8600; d(CCCGGG) = 5260; d(TACGTA) = 6300.

Poly(dG-dC), poly(dA-dT), and salmon sperm DNA were purchased from Pharmacia and used without further purification. The following ϵ_{260} (M^{-1} cm^{-1}/base) were used: poly(dG-dC) = 8400; poly(dA-dT) = 6600. An $\epsilon_{260}{}^{1mg} = 20$ was used for salmon sperm DNA.

Computational Procedure. As in our preceding studies devoted to the interactions of intercalator−oligopeptide conjugates with DNA *(10, 41, 43, 44, 75, 76)*, the computations were performed with the JUMNA molecular mechanics procedure *(77, 78)*. The standard calibration of the method was used. As discussed in the original papers, solvation effects were implicitly accounted for by the use of a sigmoidal dielectric function, and, to account for screening effects, the phosphodiester group had a net charge of −0.5. We followed a similar strategy as previously described *(44, 76)* consisting of (a) using JUMNA, creation of an intercalation site at the $d(CpG)_2$ site of the oligonucleotide with an interplanar separation of 6.8 Å; (b) manual docking of the ligand using the BioSym graphics software (BioSym Tech-

nologies, 9685 Scranton Road, San Diego, CA). This was done by inserting the porphyrin ring in the intercalation site, while each of the *N*-methylpyridinium rings was located in the appropriate groove according to the binding model considered, whether A, B, or C described below; (c) one round of restrained energy-minimization, in which hydrogen-bonding distances are imposed between the guanidinium group of the arginine side-chain and the appropriate sites (O_6 and N_7 of guanines for sequences **1** and **2**; O_2 of thymines and N_3 of adenines for the minor groove of sequence **3**, O_4 of thymines and N_7 of adenines for its major groove) belonging to the two successive base-pairs flanking the intercalation site on both DNA strands; (d) unconstrained energy-minimization using the restrained mininum-energy position as a starting point. Further details are reported in ref 44.

UV−Visible Spectroscopy. Titration. The titration experiments were performed by measuring the ligand absorption at the Soret maximum band in the visible spectral region. The complexation of the ligand was followed by adding increasing amounts of DNA at $1 \leqslant 1/r_0 \leqslant 20$, ($1/r_0$ is the ratio of the initial concentrations $[DNA]_0(bp)/[ligand]_0$) from 10 mM sodium cacodylate buffer (pH 7) and 100 mM NaCl solutions. The titration experiments for all the duplexes were carried out at room temperature except for d(ATTACGTAAT)$_2$ and d(GTTACGTAAC)$_2$ which were performed at 15 °C and for d(TACGTA)$_2$ at 5 °C. *Helix−Coil Transition.* Melting curves were recorded with a Kontron Uvikon 942 spectrophotometer. Temperature of the cell holder was varied (0.15 °C/min) by circulating water using a Huber water bath, controlled by a Huber PD415 temperature programmer. For these experiments, oligonucleotides were dissolved in 10 mM sodium cacodylate buffer (pH 7), 100 mM NaCl, at a 70 μM/phosphate concentration. The melting of the free duplexes was followed by monitoring the absorbance at 260 nm. The thermal denaturation profiles of the complexes were monitored both at 260 nm and at two wavelengths corresponding to the absorption of bound and free ligand, respectively. Melting temperatures (T_m) were determined from the first derivative of the melting curves.

Circular Dichroism. Circular dichroism spectra were recorded in a 20 °C thermostated room on a Jobin Yvon CD6 autodichrograph. All the measurements were made in 10 mM sodium cacodylate buffer (pH 7). We used a 3 mL, 10 mm path length quartz cuvette to avoid dichroic effect with the cuvette. Porphyrin and oligonucleotide concentrations were 3.3×10^{-6} M and 3.3×10^{-5} M, respectively ($1/r_0 = 10$). All spectra were obtained by an average of four accumulations recorded with steps of 0.2 nm and a response time of 0.5 s. For each measurement, the spectrum of the porphyrin at the same concentration in the same buffer and same cuvette was subtracted. The observed Δ(OD) was divided by the initial porphyrin concentration, giving apparent $\Delta\epsilon$ values, $\Delta\epsilon_{app}$.

Vibrational Spectroscopy. FTIR spectra were recorded using a Perkin-Elmer 2000 spectrophotometer. Twenty scans were usually accumulated. FTIR spectra were treated with the Galaxy Grams 386 program. These treatments include the multiple point baseline correction.

The interaction of the ligands with the duplexes was studied at physiological pH, with increasing ligand/DNA ratio, r_0, from 1/30 to 1/5. The spectra of the ligands were subtracted from the spectra of the complexes, using the BAP bands at 1730 and 1170 cm^{-1} or the H_2TMPyP-4 bands at 1185 and 800 cm^{-1}. These ligand bands exhibited no major alteration and were isolated from the DNA bands.

The sample solutions were deposited between ZnSe windows (pH ~ 7) at a concentration of 170 mM per base pair. Deuteration experiments were performed by drying the samples under nitrogen and redissolving in D_2O. All IR spectra were recorded at room temperature except the d(TACGTA)$_2$ spectra which were recorded at 5 °C. The temperature was monitored using a Specac temperature controller.

As the hexamers exhibit better-resolved spectra than the other oligonucleotides, we have restricted the presentation of the spectra to the hexamers alone and in interaction with BAP and H_2TMPyP-4.

RESULTS AND DISCUSSION

Molecular Modeling

For both major and minor groove binding, three distinct modes of binding of BAP were compared: mode A, with the phenyl group (bearing the arginyl arms) in one groove and the three *N*-methylpyridinium rings in the opposite groove; mode B, with the phenyl group and the two *N*-methylpyridinium rings flanking it in the same groove, while the third *N*-methylpyridinium ring is in the opposite groove; mode C, with the phenyl group and one of the *N*-methylpyridinium rings flanking it in the same groove, while the other two *N*-methylpyridinium rings are in the opposite groove.

Several DNA dodecameric sequences were investigated, all having in common a d(C^5pG^6)·d($C^{7'}pG^{8'}$) site, where the chromophore is intercalated. Our discussion of the theoretical results below is limited to the three sequences: **1**, d(GTGGC GCCCGAA)·d(TTCGGGC GCCAC), the HIV PBS sequence; **2**, d(GTCCC GGGCGAA)·d(TTCGCCC GGGAC); **3**, d(GTTAC GTACGAA)·d(TTCGTAC GTAAC). Sequence **2** differs from sequence **1** by a permutation of the G and C belonging to the two base pairs immediately adjacent to the intercalation site. Such a permutation will enable us to evaluate the sensitivity of the binding energy of BAP to the location of the targeted guanines, whether upstream (as in **1**) or downstream (as in **2**) from the intercalation site. Sequence **3** differs from sequence **1** by replacing these G and C bases by A and T ones, respectively, enabling us to compare the strength of the arginine−guanine interactions in the major groove to the strength of the arginine−adenine/thymine ones in both grooves. Because mode A was computed to be the best binding mode of BAP in either groove, our results are limited to this mode. A more detailed account, comparing these three sequences to several additional candidates, and the binding energies of BAP in modes A−C, will be published separately. Base numbering of the double-stranded dodecamers is given in Figure 2.

A. Major Groove Binding. The results of our computations are reported in Table 1, which lists, for the three investigated sequences the intermolecular DNA−BAP interaction energy E_{int}; the values of the DNA, ΔE_{DNA}, and ligand, ΔE_{ligand}, conformational energy changes with respect to their preferred conformational energies in the absence of

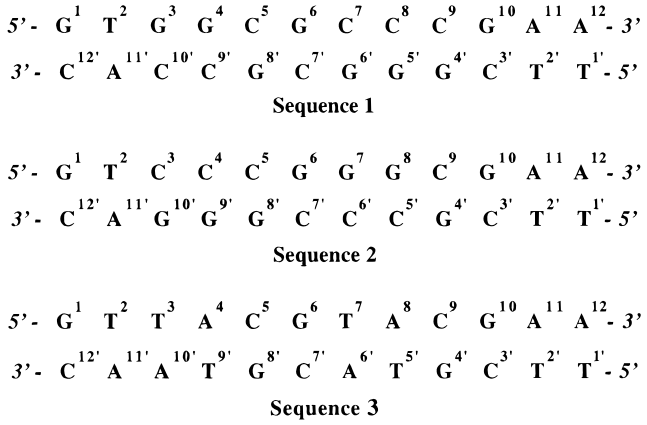

FIGURE 2: Base numbering of the three double-stranded DNA dodecamers investigated for the binding of BAP. Upper line: the "Watson" strand along the 5′→3′ direction. Lower line: the "Crick" strand along the 3′→5′ direction.

Table 1: Binding Energies (kcal/mol) of Bis(arginyl)porphyrin BAP with Oligonucleotides: d(GT**GGC GCC**CGAA)·d(TTCG**GGC GCC**AC), (HIV PBS Sequence); d(GT**CCC GGG**CGAA)·d(TTCG**CCC GGG**AC); d(GT**TAC GTA**CGAA)·d(TTCG**TAC GTA**AC)

	binding of arginyl arms to target site			
	in the major groove:			in the minor groove:
	GGC GCC	CCC GGG	TAC GTA	TAC GTA
E_{int}	−327.0	−301.4	−293.0	−257.0
ΔE_{DNA}	104.4	79.6	83.8	61.0
ΔE_{ligand}	14.6	21.1	16.0	17.3
$\Delta E = E_{int} + \Delta E_{DNA} + \Delta E_{ligand}$	**−208.0**	−200.7	−193.2	−178.7
$\delta\Delta E$	0	7.3	14.8	29.3

interaction; the resulting energy balance ΔE; and the difference, δ, of energy balances, with respect to the best value of ΔE taken as energy zero.

Table 1 indicates the following:

(1) The most stable complex is the one with sequence **1**, the targeted HIV site, encompassing the palindrome d(GGC GCC)$_2$ with two guanines upstream from the intercalation site. It is 7.3 and 14.8 kcal/mol more stable than sequences **2** and **3**, respectively.

(2) A significant energy preference occurs in favor of the major groove binding, as the minor groove complex of BAP with sequence **3** is 14.5 kcal/mol less stable than the corresponding major groove complex, and 29.3 kcal/mol less stable than the best major groove complex.

Mode A complexes are stabilized by close (3 Å) electrostatic interactions between the quaternary nitrogen of the two *N*-methylpyridinium rings flanking the phenyl group and the oxygen O_2 of two phosphate groups belonging to both DNA strands. Thus, in the complex of BAP with sequence **1**, four such interactions can be characterized. The first two involve O_2 of a phosphate connected by its $O_{3'}$ ester oxygen to $C^{7'}$ of the intercalation site on the primed strand, and O_2 of the phosphate connected through $O_{3'}$ to the cytosine base C^8, two steps downstream from the intercalation site. The other two involve the other *N*-methylpyridinium nitrogen with, on one hand, O_2 of the phosphate connected through $O_{3'}$ to the cytosine base $C^{10'}$, two steps downstream from the intercalation site; and, on the other hand, O_2 of the phosphate connected through $O_{3'}$ to the other cytosine base C^5 of the intercalation site, now on the unprimed strand.

Consideration of the structures of representative complexes sheds light on the factors governing these energetical orderings. The list of the intermolecular ligand−DNA H-bonds of the representative complexes is reported in Table 2. Additional data and the Cartesian coordinates of these complexes are available upon request.

The complex of BAP with sequence **1** is represented in Figure 3. On the first arginyl arm, two amino protons of the guanidinium group, H_c and H_d, bind, respectively, to N_7 and O_6 of the two successive guanines G^3 and G^4, located two steps and one step upstream from the intercalation site. Another amino proton of the guanidinium group, H_b, is also able to span N_7 of G^3 through an elongated H-bond. Interactions of an arginine side-chain with two successive guanines were recently observed in the crystal structure of the complex of the DNA-binding domain of yeast RAP1 with a telomeric DNA *(39)*. The amino proton H_e, cis to H_d, is simultaneously H-bonded to both N_7 and O_6 of base $G^{8'}$ of the intercalation site on the other strand of DNA. The amino proton H_d and the amide proton of the arginine are also H-bonded to O_6 of $G^{8'}$. On the second arginyl arm, two amino protons of the guanidinium group, $H_{c'}$ and $H_{d'}$, bind, respectively, to N_7 and O_6 of the two successive guanines $G^{5'}$ and $G^{6'}$, upstream from the intercalation site. The amino proton $H_{e'}$ binds not only to N_7 of $G^{6'}$, but also to O_6 of base G^6 of the intercalation site on the other strand of DNA. Additional intermolecular interactions involve the amino proton $H_{b'}$ with O_1P belonging to $G^{4'}$, three steps upstream from the intercalation site and the amide proton of the arginine with O_6 of G^6.

Replacement of G^3-G^4/$G^{5'}$-$G^{6'}$ by cytosines to yield sequence **2** with a hexameric palindrome d(CCC GGG)$_2$ results in a 7.3 kcal/mol loss in the total binding energy. The ligand−DNA intermolecular interaction energy is much less favorable (25.6 kcal/mol) than with the PBS sequence, but this is compensated by a much smaller (24.8 kcal/mol) DNA conformational energy loss, counteracted, however, by a more costly (6.5 kcal/mol) ligand conformational energy. The complex is stabilized by a much more localized array of H-bonds, limited to N_7 and O_6 of guanines G^6 and $G^{8'}$ of the intercalation site and of guanines G^7 and $G^{9'}$ one step downstream from the intercalation site (see Table 2).

Replacement of G^3-G^4/$G^{5'}$-$G^{6'}$ by T^3-A^4/$T^{5'}$-$A^{6'}$ to yield sequence **3** with a hexameric palindrome d(TAC GTA)$_2$ results in a greater (14.8 kcal/mol) loss of the binding energy. Although the E_{int} value is the weakest one among mode A major groove complexes, it is compensated to some extent by a smaller DNA conformational energy loss. In addition to the H-bonds of arginine with G^6 and $G^{8'}$ of the intercalation site common to the other sequences, the complex is stabilized by two H-bonds between the first arginine side-chain and O_4 of T^3 and $T^{9'}$ across the major groove and one H-bond between the second arginine side-chain and N_7 of $A^{6'}$ (see Table 2).

These major groove complexes are characterized by large DNA deformation energies. These ΔE_{DNA} values are in the range of those found in a theoretical study of the major groove binding of a proline-rich derivative of 9-aminoacridine *(44)*. The BAP complex with sequence **1** has the

Table 2: Values of the Ligand−Oligonucleotide Distances (Å) in the Optimized Complexes of Bis(arginyl)porphyrin BAP with Sequences: 1: d(GT**GGC GCC**CGAA)·d(TTCG**GGC GCC**AC), (HIV PBS Sequence); 2: d(GT**CCC GGG**CGAA)·d(TTCG**CCC GGG**AC); 3: d(GT**TAC GTA**CGAA)·d(TTCG**TAC GTA**AC)

binding of arginyl arms			
in the major groove:			
sequence 1	sequence 2	sequence 3	in the minor groove: sequence 3
First Arginyl Arm H-Bonds			
$H_b-N_7(G^3)$ 2.8	$H_b-O_6(G^{9'})$ 2.1		$H_a-O_{1'}(C^5)$ 2.1
$H_c-N_7(G^3)$ 2.0	$H_c-N_7(G^{9'})$ 2.0	$H_c-O_4(T^3)$ 2.3	$H_b-N_3(A^4)$ 2.3
$H_d-O_6(G^4)$ 2.2	$H_d-N_7(G^{8'})$ 2.5	$H_d-O_4(T^{9'})$ 1.9	$H_c-N_3(A^{10'})$ 2.1
$H_d-O_6(G^{8'})$ 2.0			$H_d-O_{1'}(A^{10'})$ 2.0
$H_e-N_7(G^{8'})$ 2.2	$H_e-N_7(G^{8'})$ 2.2		
$H_e-O_6(G^{8'})$ 2.3		$H_e-O_6(G^{8'})$ 1.9	
$H_f-O_6(G^{8'})$ 2.6	$H_f-N_7(G^{8'})$ 2.8	$H_f-O_6(G^{8'})$ 2.7	
Second Arginyl Arm H-bonds			
$H_{b'}-O_1P(G^{4'})$ 1.9	$H_{b'}-O_6(G^7)$ 2.1		$H_{a'}-O_{1'}(C^9)$ 2.0
$H_{c'}-N_7(G^{5'})$ 2.3	$H_{c'}-O_6(G^7)$ 2.1		$H_{b'}-O_2(C^9)$ 2.2
$H_{d'}-O_6(G^{6'})$ 1.9	$H_{d'}-N_7(G^6)$ 2.8	$H_{d'}-O_6(G^6)$ 2.0	$H_{c'}-O_2(T^{5'})$ 2.1
$H_{e'}-N_7(G^{6'})$ 2.6	$H_{e'}-N_7(G^6)$ 2.1	$H_{e'}-N_7(G^6)$ 2.1	$H_{d'}-N_3(A^{6'})$ 2.1
$H_{e'}-O_6(G^6)$ 2.3	$H_{e'}-O_6(G^6)$ 2.4	$H_{e'}-N_7(A^{6'})$ 2.1	
$H_{f'}-O_6(G^6)$ 2.1	$H_{f'}-O_6(G^6)$ 2.0		$H_{f'}-O_2(C^{7'})$ 2.0
$O_{g'}-H_2(N_4)$ $(C^{7'})$ 2.0			
Ionic Interactions			
N_A-O_2P (C^5) 3.3	N_A-O_2P (C^5) 3.5	N_A-O_2P (C^5) 3.3	N_A-O_1P (C^5) 3.5
N_A-O_2P $(C^{10'})$ 3.6	N_A-O_2P $(G^{10'})$ 3.0	N_A-O_2P $(A^{10'})$ 3.8	
N_C-O_2P (C^8) 2.9	N_C-O_2P (G^8) 3.0	N_C-O_2P (A^8) 2.8	
N_C-O_2P $(C^{7'})$ 3.0	N_C-O_2P $(C^{7'})$ 3.3	N_C-O_2P $(C^{7'})$ 3.1	N_C-O_1P $(C^{7'})$ 3.2

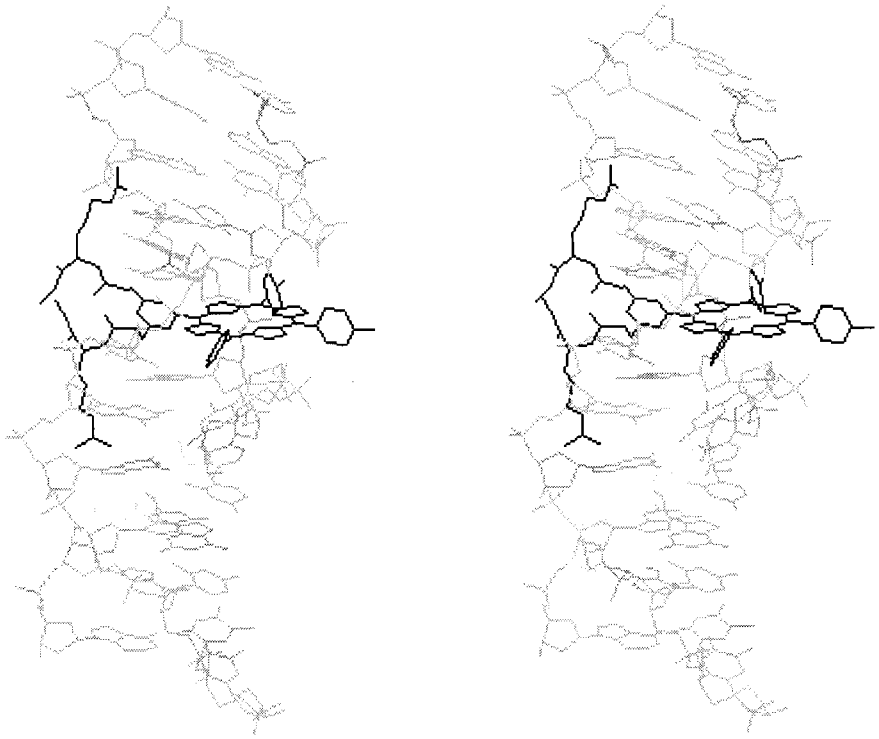

FIGURE 3: Stereoview of the major complex of BAP with sequence d(GTGGCGCCCGAA)·d(TTCGGGCGCCAC). (Hydrogens are omitted for clarity).

greatest number of hydrogen-bond interactions and is also the one having the highest ΔE_{DNA} value. This could reflect the onset of more extensive DNA conformational rearrangements induced by the arginine arms. We have compared the values of the DNA torsional angles in these three complexes (available upon request). Comparable values were found in the BAP complexes with sequences **2** and **3**. The BAP·**1** complex had a similar pattern of torsional angles as BAP·**2**, except for base $G^{8'}$, with ϵ and ζ torsional angles that are g^- and *t*, respectively, instead of the reverse situation with the BAP·**2** complex. Finally we note that the sugar pucker pattern is $C_{2'}$ endo for the four bases of the intercalation site, except with the BAP·**3** complex, for which the sugars of bases G^6 and $G^{8'}$ are $C_{1'}$ exo.

Overall, the PBS-encompassing sequence was thus predicted to have the best binding energy for BAP. Similar results were obtained in mode B (Gresh and Perrée-Fauvet, to be published).

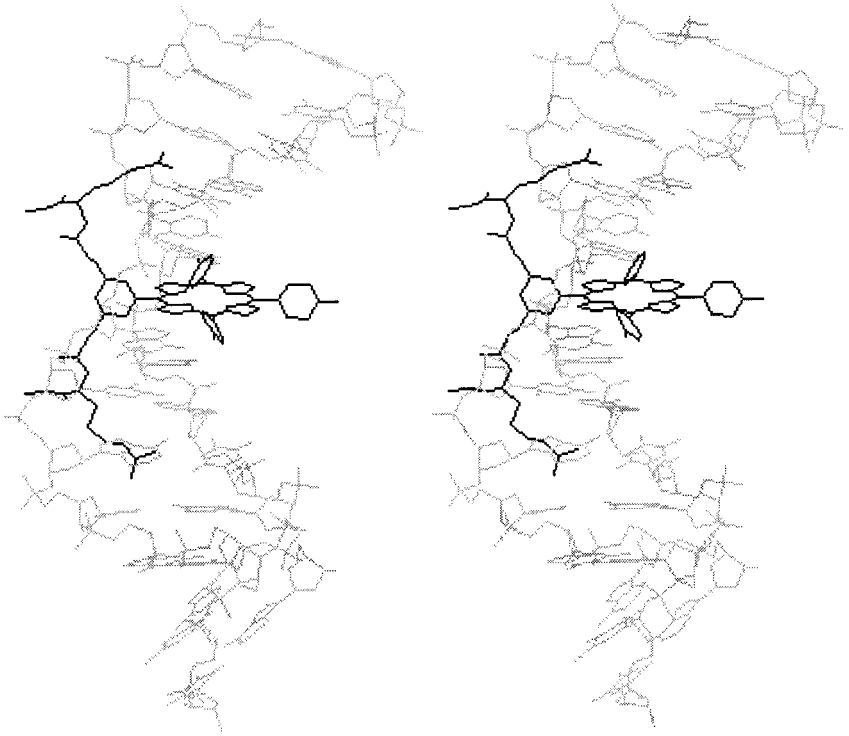

FIGURE 4: Stereoview of the minor complex of BAP with sequence d(GTTACGTACGAA)·d(TTCTAGCGTAAC). (Hydrogens are omitted for clarity).

B. Minor Groove Binding. Investigation of minor groove binding was restricted to sequence **3** with the hexameric palindrome $d(TACGTA)_2$, on account of the more attractive electrostatic potential exerted on positive charge(s) in the minor groove by AT-rich sequences than by GC-rich ones *(79)*. The results of the computations are reported in Table 1 along with those of the major groove. The complex of BAP is represented in Figure 4. Comparison with the energy of complexation with sequence **1** in the major groove shows a very great energy difference in terms of E_{int} (70 kcal/mol), compensated by a much smaller (by 43 kcal/mol) DNA conformational energy term. Minor groove binding in mode A is in fact the one giving rise to the smallest DNA conformational energy rearrangement, namely 61 kcal/mol.

The minor groove complex of BAP in mode A is stabilized by H-bonds between each arginine side-chain and N_3, O_2, and $O_{1'}$ sites, with the guanidinium group cross-linking both DNA strands (see Table 2). A similar pattern was observed in the theoretical study of the minor groove complexes of a proline-rich derivative of 9-aminoacridine *(44)*. In addition and similar to the situation found with BAP, the minor groove binding of this derivative led to smaller DNA deformation energies than its major groove binding. The ΔE_{DNA} value is smaller in the case of the minor groove BAP complex, but it is in the range of values found in a theoretical study of the binding of a porphyrin−netropsin derivative to double-stranded B-DNA dodecamers *(76)*. The conformational changes are more localized in the vicinity of the intercalation site than in the BAP major groove complexes. This could provide an explanation for the fact that the ΔE_{DNA} value is smaller than in the latter complexes. In addition, the intercalation site has the more standard mixed sugar pucker pattern, instead of the uniform one found in the major groove complex.

UV−Visible Spectroscopy

All spectroscopic measurements were performed on DNA sequences having the same palindromic hexamers as the sequences **1**, **2**, and **3**, namely, $d(GGCGCC)_2$, $d(CCCGGG)_2$, and $d(TACGTA)_2$, respectively.

Visible Titration at the Soret Band of the Porphyrins. Typical absorption titration curves for the binding of BAP to $d(GGCGCC)_2$ and $d(TACGTA)_2$ are given in Figures 5a and 5b, respectively. Table 3 reports the absorption changes at the Soret maximum band of BAP upon interaction with all the investigated oligonucleotides. Large hypochromicities ($H = 40-43\%$) and substantial red shifts ($\Delta\lambda = 19-21$ nm) of the Soret maximum band are observed upon interaction with GC-rich oligonucleotides. Interaction of BAP with AT-rich oligonucleotides induces slightly weaker changes: a smaller ($\Delta\lambda = 15$ nm) bathochromic shift upon interaction with $d(TACGTA)_2$, and a smaller ($H = 33-35\%$) hypochromicity in the presence of the two AT-rich decamers.

We correlated our UV−visible results with those obtained in studies of the complexes formed between H_2TMPyP-4 and its analogues, with polynucleotides *(12, 13, 72, 80−83)*. These studies have demonstrated that H_2TMPyP-4 binds by intercalation in GC regions whereas in AT regions it forms nonintercalated complexes which could involve electrostatic interactions with the phosphate backbone as well as groove binding. Such preferences could be accounted for by molecular mechanics calculations *(84)*. The intercalation mode was characterized by a substantial (>15 nm) bathochromic shift and a strong (>35%) hypochromicity of the Soret band, and the nonintercalated binding mode, by a small red shift and a low hypochromicity *(72)*. For that purpose, we extended our UV−visible study to the complexes of BAP with the poly(dG-dC) and poly(dA-dT) polynucleotides, as well as to salmon sperm DNA, which has an intermediate

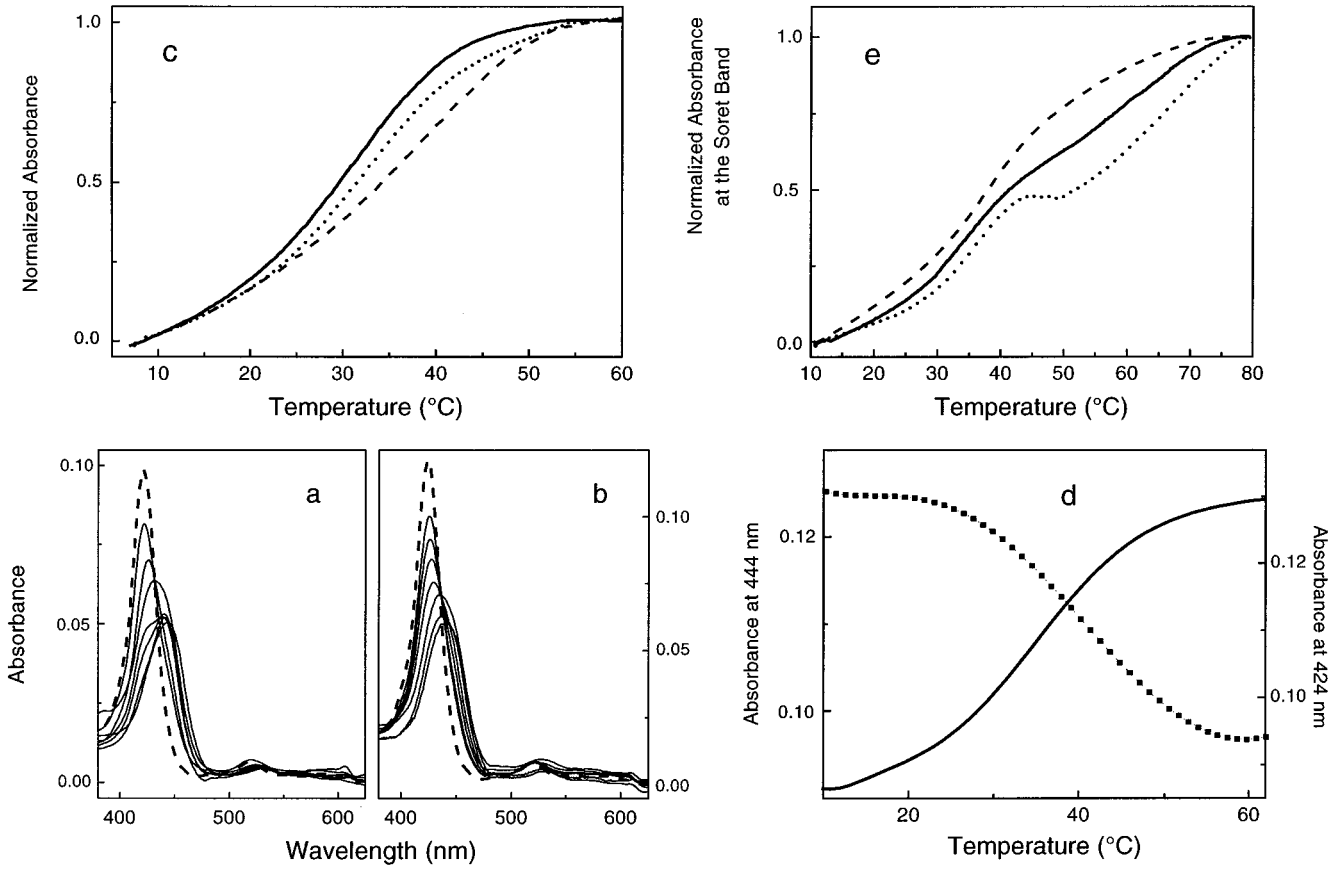

FIGURE 5: Absorption titration of BAP with (a) d(GGCGCC)$_2$: (---) no DNA. (—) ligand in the presence of DNA ($1/r_0$ = 1.4 to 20); (b) d(TACGTA)$_2$: (---) no DNA, (—) ligand in the presence of DNA ($1/r_0$ = 1.4 to 20); (c) Normalized melting curves of (—) d(GGCGCC)$_2$, (---) d(GGCGCC)$_2$·BAP, (···) d(GGCGCC)$_2$·H_2TMPyP-4; (d) denaturation profiles of BAP in d(GGCGCC)$_2$·BAP: (—) absorbance at 424 nm, (■) absorbance at 444 nm, at $1/r_0$ = 10; (e) denaturation profiles of the Soret maximum band of BAP or H_2TMPyP-4 in complexation with d(GTTACGTAAC)$_2$: (---) BAP at $1/r_0$ = 10, (—) BAP at $1/r_0$ = 5 and (···) H_2TMPyP-4 at $1/r_0$ = 10.

Table 3: Spectroscopic and Thermodynamic Data of the Nucleic Acids upon Interaction of BAP and H_2TMPyP-4[a,b]

		complex with BAP				complex with H_2TMPyP-4			
DNAs	T_m^{260} (°C) (±1)	Δλ (nm)	H%	T_m^{260} (°C) (±1)	T_m^{424}(°C) (±1)	Δλ (nm)	H%	T_m^{260} (°C) (±1)	T_m^{421} (°C) (±1)
poly(dG-dC)	–	21	40	–	–	22	40	–	–
poly(dA-dT)	–	8	7	–	–	9	7	–	–
salmon sperm DNA	–	11	39	–	–	11	39	–	–
d(GT**GGC GCC**GAA)· d(TTCG**GGC GCC**AC)	59	20	40	62	63	20	40	60	70
d(**GGC GCC**)$_2$	31	20	43	39	37	19	41	34	43
d(**CCC GGG**)$_2$	31	19	42	32	33	21	42	34	43
d(**TAC GTA**)$_2$	12	15	39	13	12	21	41	17	25
d(GT**GGC GCC**AC)$_2$	56	21	42	60	62	20	41	57	65
d(GT**CCC GGG**AC)$_2$	50	19	41	51	53	20	40	53	61
d(AT**TAC GTA**AT)$_2$	26	20	33	27	29	20	38	35	26, 47
d(GT**TAC GTA**AC)$_2$	33	20	35	35	36	21	39	43	34, 57

[a] The titration results given in this table as well as all the denaturation experiments are recorded at $1/r_0$ = 10. [b] Bathochromic shift (Δλ) is defined as $\lambda_f - \lambda_b$ where λ_f = absorption wavelength of the free ligand and λ_b = absorption wavelength of the ligand in the presence of DNA. Hypochromicity (H%) is defined as $\{(A_f - A_b) \times 100\}/A_f$; where A_f = absorption of the ligand solution at λ_f and A_b = absorption of the same concentration of the ligand in the presence of DNA at λ_b.

content in G−C base pairs. The complexes of H_2TMPyP-4 with the oligo- and polynucleotides were investigated in parallel to evaluate whether the introduction of the arginine side-chains could interfere with such distinct preferences of the porphyrin ring.

Table 3 shows that both ligands present the same spectroscopic behavior upon interaction with poly(dG-dC), poly(dA-dT), and salmon sperm DNA. The data are consistent with the above-mentioned studies on H_2TMPyP-4 with the polynucleotides. The complexes of salmon sperm DNA present an intermediate bathochromic shift, and a very similar hypochromicity to that of poly(dG-dC). This confirms that BAP, like H_2TMPyP-4, forms intercalated complexes with GC-rich DNAs, and nonintercalated complexes with AT-rich ones. Thus, additional interactions of the two arginine side-chains at GC-rich sites did not occur at the

expense of the intercalation of the porphyrin ring. In their complexes with the GC-rich oligonucleotides, both ligands display similar spectral changes, which are close to those found with poly(dG-dC). The bathochromic shifts and hypochromicities of the complexes of H_2TMPyP-4 with the TACGTA-containing duplexes are only slightly greater than those of BAP. *Overall, the high values of the hypochromicity and red shift observed upon interaction of BAP and H_2TMPyP-4 with all duplexes indicate that an intercalation binding mode is taking place in the complexes of both BAP and H_2TMPyP-4 with all the oligonucleotides.*

Thermal Denaturation. The values of the melting temperatures of the free and complexed oligonucleotides, as monitored by the change of the absorption maximum at 260 nm, are reported in Table 3. Figure 5c shows the representative denaturation profiles of the d(GGCGCC)$_2$ hexamer, free, and in its complexes with BAP or H_2TMPyP-4. Complexation by BAP resulted in a notable stabilization of the double helix, as translated by a ΔT_m^{260} of +8 °C. *In marked contrast, the complexes of BAP with the other two hexamers, d(TACGTA)$_2$, (the "AT- rich"* one) and d(CCCGGG)$_2$ *(the "isomeric sequence")* produce a virtually negligible gain in double helix stabilization, as translated by ΔT_m^{260} values of 1 °C. The amount of ligand-induced thermal stabilization decreases upon increasing the length of the oligonucleotides, as these melt at increasingly higher temperatures, whereas the number of available binding sites is constant. Thus, $\Delta T_m^{260} = 4$ °C for the PBS-encompassing sequence dodecanucleotide, which melts at 59 °C instead of at 31 °C for the corresponding hexamer. These thermal denaturation data on the complexes of BAP clearly indicate its preferential binding to sequences encompassing d(GGCGCC)$_2$ and are in full agreement with the theoretical predictions. On the other hand, the ΔT_m values for such sequences, which do not exceed 8 °C, are lower than those found when oligonucleotides are complexed by rigid groove-binders such as netropsin or distamycin *(85)* or by bisintercalators such as ditercalinium *(86, 87)*, which are in the 15−25 °C range. This translates a reduced binding affinity of BAP, as compared to these drugs, probably due to the flexibility of the arginine arms and the reduction of their conformational freedom upon complexation. Such an entropy loss could reduce the enthalpy gain due to the hydrogen-bonding interactions of the arms in the groove. We are presently trying to increase the binding affinity by designing and synthesizing derivatives of BAP having a more structured oligopeptide backbone, and linking the C-terminal ends to an intercalator (Kossanyi et al., work in progress).

It is noteworthy that, lacking the arginine side-chains, H_2TMPyP-4 appears to be indiscriminatory between the d(GGCGCC)$_2$ hexamer and its d(CCCGGG)$_2$ isomer, since its binding to either one results in an identical and much weaker amount of thermal stabilization ($\Delta T_m^{260} = 2-3$ °C). When H_2TMPyP-4 interacts with the AT-rich hexamer, d(TACGTA)$_2$, the amount of thermal stabilization is now slightly higher ($\Delta T_m^{260} = 5$ °C) which can be ascribed to the onset of a nonintercalated binding mode of H_2TMPyP-4. We also note that, in these H_2TMPyP-4 complexes, ΔT_m^{260} increases as the length of the AT-rich oligonucleotides increases, thus reaching 9 and 10 °C with the double-stranded d(ATTACGTAAT)$_2$ and d(GTTACGTAAC)$_2$ decamers. This could be due to the increase of the AT binding sites available in these oligomers.

In addition to the oligonucleotide thermal behavior, we also studied that of the BAP ligand by monitoring its absorbance at two wavelengths corresponding to the Soret absorption band of the free BAP ($\lambda = 424$ nm), and the bound BAP ($\lambda = 439-445$ nm, depending on the oligonucleotide). Figure 5d presents the profile of the Soret maximum band of BAP at 424 and 444 nm, in its complex with d(GGCGCC)$_2$, and in the 10−65 °C range. Increasing the temperature results in a decrease in the 444 nm and a concomitant increase in the 424 nm absorptions. The T_m^{424} values derived from the absorption band of BAP for the various BAP complexes are reported in Table 3. These values are quite similar to the corresponding T_m^{260} ones. This indicates that the dissociation of BAP occurs simultaneously with the melting of the double helix and suggests that both DNA strands are involved in binding the arginine side-chains, consistent with the theoretical model. This mechanism does not appear to prevail in the case of the H_2TMPyP-4 complexes. Table 3 shows that their T_m^{421} values can be higher than those of T_m^{260}, which could denote the ability of H_2TMPyP-4 to bind to a single DNA strand, after the melting of the duplex has occurred. This is consistent with the results of previous studies by Fiel et al., Pasternack et al., and Bustamante et al., which demonstrated high-affinity binding of H_2TMPyP-4 to single-stranded polynucleotides *(13, 88, 89)*. Moreover, in the complexes of H_2TMPyP-4 with d(ATTACGTAAT)$_2$ and d(GTTACGTAAC)$_2$, the profile of the Soret maximum band of H_2TMPyP-4 (at 421 nm) presents a biphasic curve which was not observed for BAP (at 424 nm) in its complexation with these sequences at the same $1/r_0$ (Table 3, Figure 5e). This thermal bimodal behavior of the Soret maximum band of H_2TMPyP-4 was observed before in the complex of this ligand with calf thymus DNA *(13)*. In line with this finding, we suggest that the low-temperature transition might represent the passage of the porphyrin from an intercalated to a nonintercalated binding mode. We have checked that when the temperature is increased to values close to the melting point of the duplexes, the profile of the Soret band displays lower hypochromicity and bathochromic shift, corresponding to a nonintercalated binding mode (data not shown). The high-temperature transition might reflect the dissociation of a partly associated complex from single-stranded DNA. This type of biphasic transition was also observed for the corresponding complexes of BAP, but at higher ligand concentrations (Figure 5e).

Circular Dichroism

Porphyrins, although nonchiral, display induced circular dichroism (CD) spectra in the Soret band region when they are bound to DNA. The appearance of a negative induced CD band is a signature for intercalation whereas a positive induced band is indicative of a nonintercalated binding mode *(72)*. Thus, in addition to UV−visible absorption measurements, a CD study is a useful tool for the diagnostic of the interaction of BAP with the oligonucleotides encompassing the GGCGCC, CCCGGG, and TACGTA hexamers.

The experiments were carried out in the presence of the three decamers d(GTGGCGCCAC)$_2$, d(GTCCCGGGAC)$_2$,

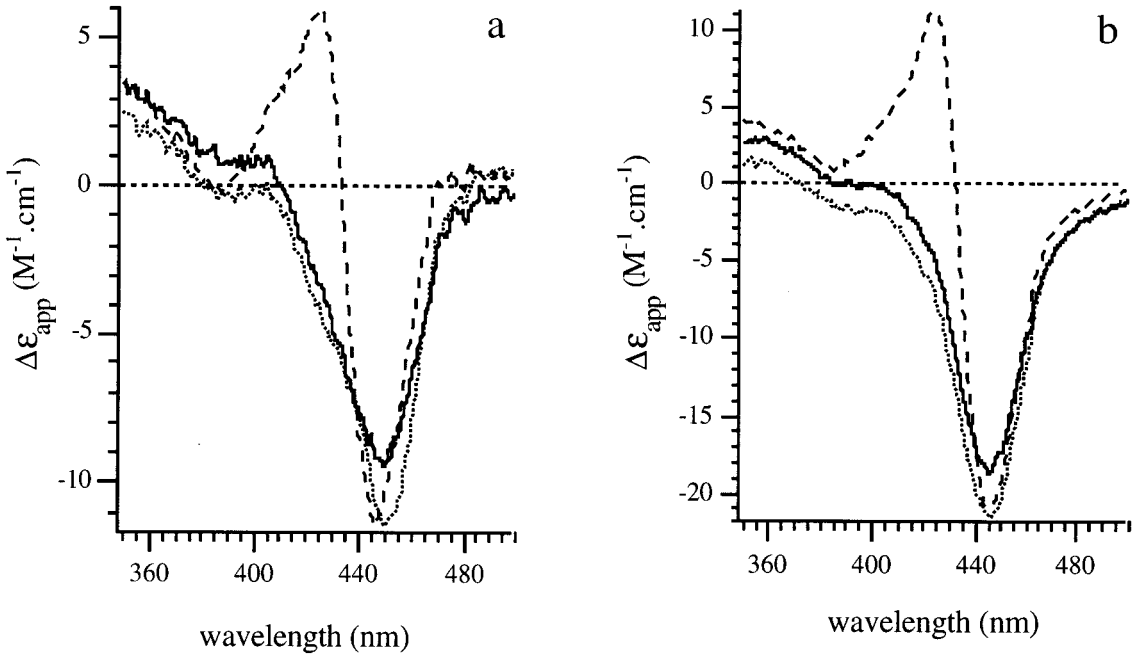

FIGURE 6: Induced CD spectra in the Soret region of (a) BAP; (b) H_2TMPyP-4; in the presence of (—) d(GTGGCGCCAC)$_2$; (···) d(GTCCCGGGAC)$_2$; (---) d(GTTACGTAAC)$_2$ at $1/r_0 = 10$.

and d(GTTACGTAAC)$_2$, which, in UV−visible spectroscopy, were seen to induce substantial hypochromicities and bathochromic shifts of the Soret band of BAP (see Table 3). Measures were performed at $1/r_0 = 10$, in the same conditions as the UV−visible spectroscopy measurements. As seen in Figure 6a, BAP displays a unique broad negative signal with the first two oligonucleotides. This is the signature of a unique binding mode of BAP by intercalation into the common central d(CpG)$_2$ site of these decamers. Upon interaction with the AT-rich decamer, BAP exhibits a different pattern: the negative band although of the same intensity, is narrower, and is accompanied by a smaller positive one, which indicates the formation of a nonintercalated complex. The same experiments were carried out with H_2TMPyP-4 which, upon interaction with these oligonucleotides, exhibited changes in hypochromicities and bathochromic shifts of the same order of magnitude as BAP (Table 3). As seen in Figure 6b, H_2TMPyP-4 displays similar patterns: in the presence of the decamer encompassing the PBS sequence and of its isomer d(GTCCCGGGAC)$_2$, a unique and intense negative band is induced, indicative of the intercalation of the porphyrin in these GC-rich duplexes, while both negative and positive bands appear in the presence of d(GTTACGTAAC)$_2$, reflecting the coexistence of intercalative and nonintercalative binding to this AT-rich oligonucleotide. The only difference with Figure 6a lies in the intensities of these bands, which are twice as high as those of BAP. This cannot be correlated, however, to the relative binding affinities of the two ligands because the ordinate is given in apparent $\Delta\epsilon$, which should take into account their individual ϵ values for each binding mode. These CD experiments confirm that the significant thermal stabilization of AT-rich oligonucleotides by H_2TMPyP-4 observed above may result from the nonintercalative binding of the tetracationic porphyrin, but do not explain why there is no stabilization in the presence of BAP, which appears to bind in a similar manner.

FTIR Spectroscopy

1750−1550 cm^{-1} Spectral Region. We have recorded in D_2O the FTIR spectra of d(GGCGCC)$_2$, poly(dG-dC), d(TACGTA)$_2$ and their complexes with BAP (Figures 7a−i). Figures 7a and 7b report, respectively, the FTIR spectra of d(GGCGCC)$_2$, free and complexed ($1/r_0 = 6$), and Figure 7c reports the spectrum of uncomplexed BAP. Let us recall that a carbonyl group with a normal double bond character gives a band near 1720 cm^{-1}. The carbonyl groups of the DNA bases, which, due to delocalization, have an enhanced single bond character, are observed at 40−70 cm^{-1} low-shifted frequencies. Thus, in the uncomplexed d(GGCGCC)$_2$ spectrum, the bands at 1683 and 1649 cm^{-1} are assigned by analogy with the spectrum of poly(dG-dC) *(90)* to the stretching vibrations of the C_6═O_6 of the guanine and of the C_2═O_2 of the cytosine, respectively. Complexation of d(GGCGCC)$_2$ with BAP produces an additional band at 1696 cm^{-1}. This new high-frequency shifted absorption can be assigned to the onset of hydrogen-bonding interactions between the guanines and the positively charged arginine side-chains. It has been already observed in two previous FTIR studies: the first is an early study by Tsuboi *(91)* which showed that protonation of O_6 resulted in an increase of the absorption wavenumber of the carbonyl group; the second study was devoted to the triple helices dG$_*$dC·dG and dC$^+{}_*$-dC·dG. A high-frequency shift of the C_6═O_6 absorption band, from 1689 to 1697 cm^{-1}, was taken as evidence for triple-helix formation through an additional hydrogen bond involving O_6 of the guanine, as a consequence of the enhancement of the localization character of the C═O double-bond, and the resulting increase of its force constant *(92, 93)*.

Figure 7e shows that the same high-frequency shift of the guanine carbonyl band occurs in the complex of BAP with poly(dG-dC). As with d(GGCGCC)$_2$, the band at 1696 cm^{-1} is absent from the spectrum of uncomplexed poly(dG-dC) (Figure 7d). *No such shift can be seen, in contrast, in the*

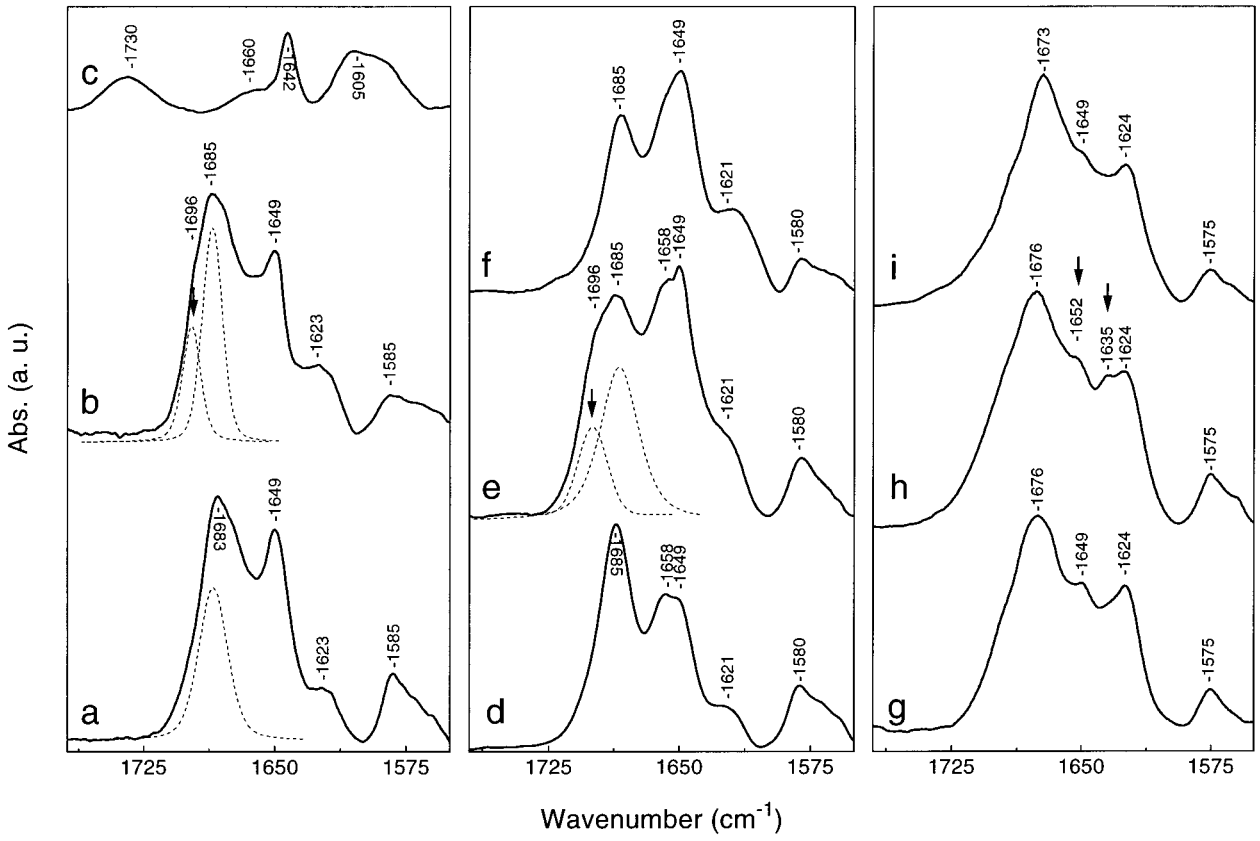

FIGURE 7: FTIR spectra (1750−1550 cm^{-1}) recorded in D_2O solution of (a) $d(GGCGCC)_2$; (b) $d(GGCGCC)_2$·BAP at $1/r_0 = 6$, after subtraction of BAP bands; (c) BAP; (d) poly(dG-dC); (e) poly(dG-dC)·BAP at $1/r_0 = 10$; (f) poly(dG-dC)·H_2TMPyP-4 at $1/r_0 = 10$; (g) $d(TACGTA)_2$; (h) $d(TACGTA)_2$·BAP at $1/r_0 = 6$; (i) $d(TACGTA)_2$·H_2TMPyP-4 at $1/r_0 = 6$; (dashed line) deconvolution bands.

complex of poly(dG-dC) with H_2TMPyP-4 (Figure 7f). This is a clear indication that the arginine side-chains are able to target the C_6═O_6 bond, and, in accordance with the theoretical predictions, *a signature for hydrogen-bonding interactions that occur in the major groove of DNA.* The presence of at least one guanine base upstream from the intercalation site (as is the case in the dG-dC-dG-dC stretch within poly(dG-dC)) appears necessary for the arginine side-chains to exert such a high-frequency shift. Indeed, this shift was not observed in the complex of BAP with the isomeric $d(CCCGGG)_2$ sequence (data not shown).

Figures 7g−i present the FTIR spectra of $d(TACGTA)_2$, free (7g) and complexed with BAP (7h) or H_2TMPyP-4 (7i) at $1/r_0 = 6$. Comparison of Figure 7g and Figure 7h shows the appearance of two absorption bands at 1635 and 1652 cm^{-1}. The band at 1635 cm^{-1} can be assigned to an unpaired thymine base. It is low-frequency shifted with respect to the 1641 cm^{-1} absorption band of paired thymine bases which can be observed in poly(dA-dT). The band at 1652 cm^{-1} can be assigned to the C_2═O_2 stretching band of an unpaired cytosine base and is high-frequency shifted with respect to the 1649 cm^{-1} absorption band of paired cytosine *(90)*. The appearance of such bands suggests that complex formation between BAP and $d(TACGTA)_2$ can result in the breaking of the hydrogen bonds between some of the bases and/or their partial unstacking. This may explain the lack of thermal stabilization in the complex with BAP. In contrast, when poly(dA-dT) (which has no intercalation sites available for cationic porphyrins) is complexed with BAP or H_2TMPyP-4, no appreciable change is detected in the spectral region of the double bond stretching vibrations of the adenines and thymines (data not shown).

1550−1250 cm^{-1} Spectral Region. Figures 8a−h monitor the spectral behavior of the N_7 site of purines, which, with O_6, constitutes the principal recognition site by electron-deficient ligands in the major groove. Figures 8a,b present the FTIR spectra of the $d(GGCGCC)_2$ hexamer, either free (8a), or in its complex with BAP (8b). The corresponding spectra of poly(dG-dC) are shown in Figures 8c and 8d, respectively and those of $d(TACGTA)_2$ in Figures 8f (free) and 8g (complexed). Finally, the spectra of the complexes of poly(dG-dC) and $d(TACGTA)_2$ with H_2TMPyP-4 are shown in Figures 8e and h. Earlier studies, which bore on poly(dG-dC), revealed by C_8−H selective deuteration that the broad band at 1498 cm^{-1} is a superposition of both cytosine and guanine absorption bands *(94)*, and that the guanine component stems from the N_7−C_8−H deformation *(95, 96)*. Modifications of the position or of the relative intensity of this band could therefore be used as a diagnostic for interactions involving N_7 of guanine. This is indeed confirmed by the low-frequency shift to 1492 cm^{-1} of this band occurring upon complexation of BAP with $d(GGCGCC)_2$ (Figure 8b) as well as with poly(dG-dC) (Figure 8d). A similar shift pattern is observed for the complex of BAP with the $d(CCCGGG)_2$ hexamer (data not shown). Such a low-frequency shift does not occur in the complex of poly(dG-dC) with H_2TMPyP-4 (Figure 8e). In line with our previous results on the C_6═O_6 absorption bands, this is an additional indication for the necessity of the arginine side-chains to target the guanines in the major groove.

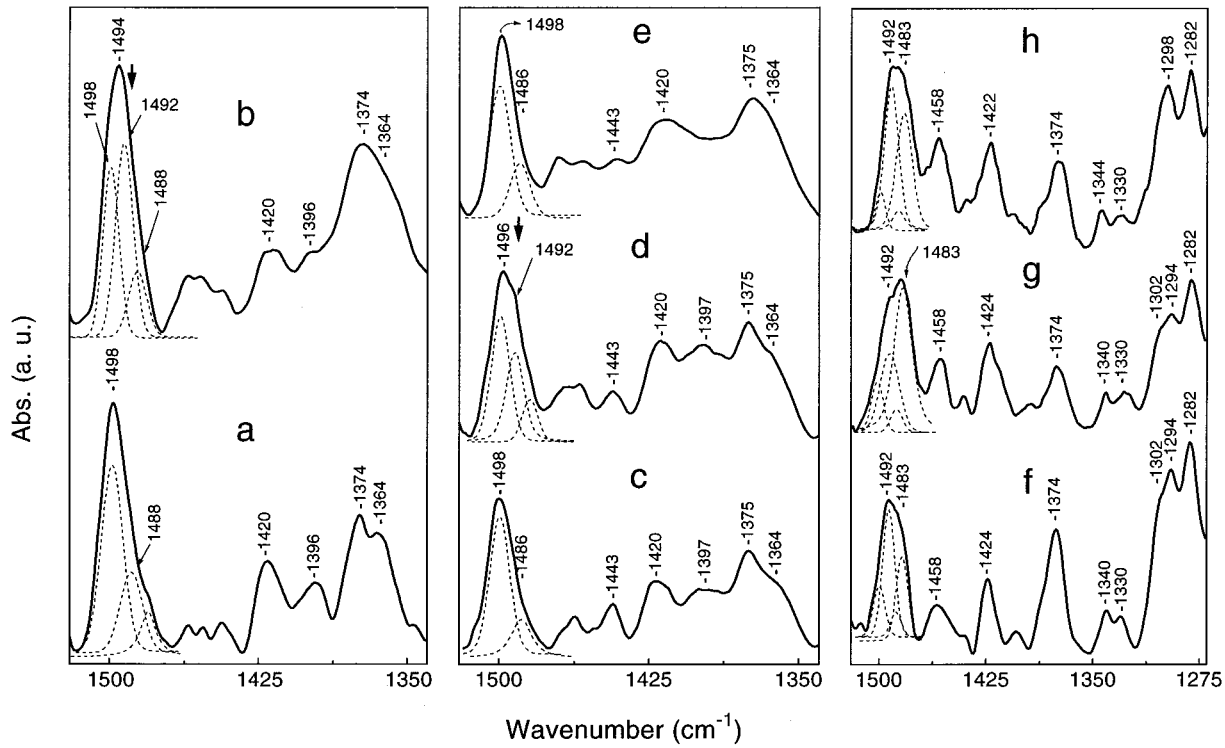

FIGURE 8: FTIR spectra (1550−1250 cm^{-1}) recorded in H_2O solution of (a) $d(GGCGCC)_2$; (b) $d(GGCGCC)_2$·BAP at $1/r_0 = 6$; (c) poly(dG-dC); (d) poly(dG-dC)·BAP at $1/r_0 = 10$; (e) poly(dG-dC)·H_2TMPyP-4 at $1/r_0 = 10$; (f) $d(TACGTA)_2$; (g) $d(TACGTA)_2$·BAP at $1/r_0 = 6$; (h) $d(TACGTA)_2$·H_2TMPyP-4 at $1/r_0 = 6$; (dashed line) deconvolution bands.

The FTIR spectrum of the free $d(TACGTA)_2$ hexamer exhibits a broad band in the 1492 cm^{-1} region with a shoulder at 1483 cm^{-1} (Figure 8f). By analogy to previous work on poly(dA-dT) *(97, 98)*, this band can be assigned to an adenine N_7-C_8-H deformation mode, partially superimposed on a thymine mode. Complex formation with BAP results in a decrease in the intensity of the 1492 cm^{-1} absorption and a concomitant increase in the intensity of the 1483 cm^{-1} low wavenumber component (Figure 8g). Such an increase at low frequency is similar to the one occurring in the complexes of BAP with $d(GGCGCC)_2$ and poly(dG-dC) (Figures 8b and 8d). It could be due to the onset of hydrogen-bonding interactions between BAP and N_7 of adenine bases. As in the case of poly(dG-dC), H_2TMPyP-4 has virtually no effect on this specific vibrational mode, as can be seen by a comparison between Figures 8f and 8h. Similar results were obtained for the complexes of BAP and H_2TMPyP-4 with poly(dA-dT) (data not shown).

The FTIR spectrum of $d(TACGTA)_2$ exhibits absorption bands at 1340 and 1302 cm^{-1} which can be assigned to N_3 adenine vibrations *(99)* (Figure 8f). The complexation of H_2TMPyP-4 results in a high-frequency shift of the 1340 cm^{-1} band and an intensity decrease in the 1302 cm^{-1} one (Figure 8h), while that of BAP causes no change. This could indicate that, in contrast to H_2TMPyP-4, BAP does not interact with N_3 in the minor groove. This is consistent with the theoretical prediction according to which, upon intercalation between the $d(CpG)_2$ sequence of the dodecamer **3**, BAP should favor major groove over minor groove binding of its arginine side-chains.

1250−1000 cm^{-1} Spectral Region. In addition to the above-mentioned groove interactions involving BAP, other interactions which take place at the level of the DNA phosphate groups have been detected in the 1250−1000 cm^{-1} spectral region. In this region, two strong bands at 1220 and 1088 cm^{-1} assigned to the antisymmetric ν_{as} and symmetric ν_s stretching vibrations of the phosphate groups and one at 1052 cm^{-1} assigned to C−O coupled to P−O stretching vibration of the DNA backbone are sensitive to phosphate groups interactions with metal cations *(100)*.

In Figures 9a−d, we observe in the spectra of BAP complexes, a new absorption band at 1067 cm^{-1}. In addition, a modification of the relative intensity of the vibrations of the phosphate groups and of the C−O bonds of the backbone is detected. Finally in the case of $d(TACGTA)_2$ (Figure 9c) and poly(dA-dT) (Figure 9d) a shift to lower wavenumbers of the ν_{as} is found.

In an earlier IR study of the interaction of free base and metalated TMPyP-4 with calf thymus DNA, a band had been detected at 1064 cm^{-1} and assigned to a shifted ν_s vibration *(101)*. The observed shifts of ν_s and ν_{as} have been interpreted as a result of ionic interactions between the positively charged groups of the porphyrin and the phosphate groups of the DNA duplex. Such ionic interactions have been proposed by Hui et al. in their theoretical models of intercalated $d(CGCGCG)_2$ and nonintercalated $d(TATATA)_2$ complexes with H_2TMPyP-4 *(84)*.

The spectral modifications observed for the different BAP complexes in Figures 9a−d suggest that the charged *N*-methylpyridinium rings of BAP interact with the phosphate groups of the DNA but in various way and to different extent depending upon the DNA sequence and the location of the porphyrin, in agreement with the theoretical models.

CONCLUSIONS

The *de novo* design of oligopeptide−intercalator conjugates, which could selectively target six to twelve base-pairs

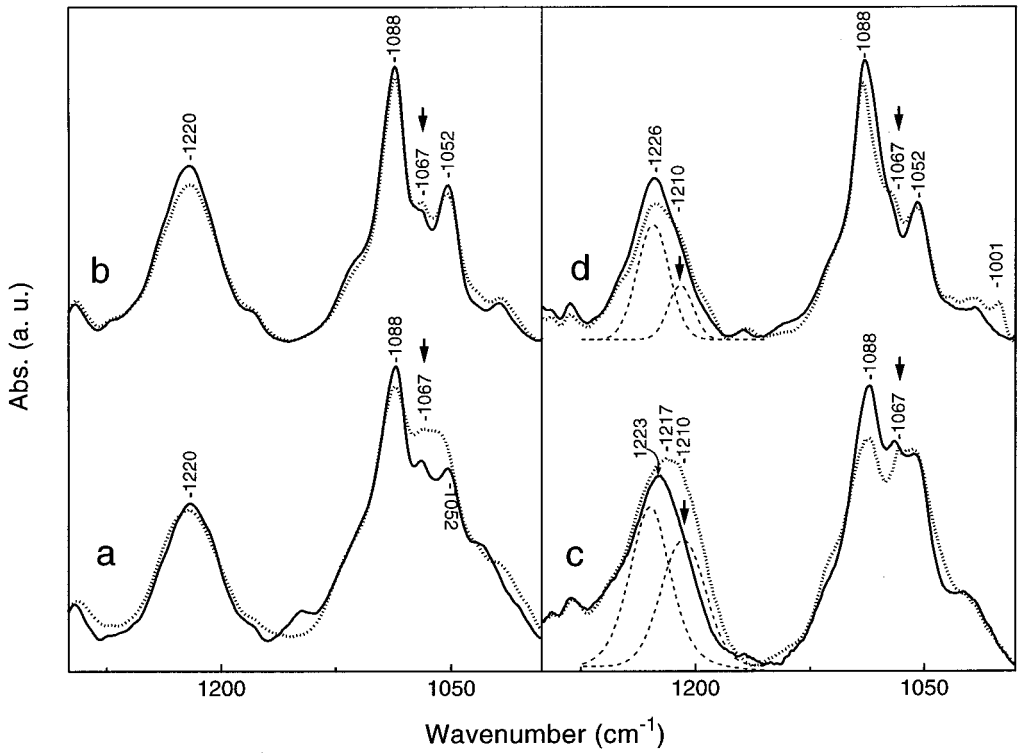

FIGURE 9: FTIR spectra (1250−1000 cm^{-1}) recorded in H_2O solution of the duplexes and their complexes with BAP: (a) $d(GGCGCC)_2$; (b) poly(dG-dC); (c) $d(TACGTA)_2$; (d) poly(dA-dT); (—) free duplexes, (•••) $1/r_0 = 6$; (dashed line) deconvolution bands. The spectra have been normalized using as internal standard the integrated area between 1160 and 995 cm^{-1}.

in the major groove of DNA, could constitute a promising alternative to triple helix formation, or to minor groove targeting by oligopeptides. To this end, we previously designed and synthesized a bis(arginyl) derivative of a tricationic derivative of H_2TMPyP-4, (BAP) *(10)* in order to target the $d(GGCGCC)_2$ sequence, which is encountered in oncogenes *(1*−*5)*, mutational hot spots *(6)*, and in the LTR sequence of the HIV-1 genome *(8, 9)*. Our theoretical calculations predicted that BAP should bind by intercalation in the middle of the $d(GGCGCC)_2$ sequence and that each arginine side-chain would bind in the major groove and form hydrogen-bonding interactions with O_6/N_7 sites belonging to two successive guanines on each strand, upstream from the intercalation site. They also predicted BAP as having a stronger affinity for this PBS-encompassing sequence than for its isomeric sequence $d(CCCGGG)_2$ and the AT-rich sequence $d(TACGTA)_2$. To validate these predictions, we resorted to the following spectroscopic techniques:

(1) UV−visible and CD spectroscopy, to provide insight on the nature of the ligand−DNA complexes, namely, whether intercalating or nonintercalating. Furthermore, we monitored the evolutions, as a function of temperature, of the DNA absorption band, and of the Soret absorption band of the ligand. This enabled us to derive the values of the DNA melting temperature and to quantify the extent of stabilization due to ligand complexation.

(2) FTIR spectroscopy, to monitor the behavior of the $C_6{=}O_6$ and $N_7{-}C_8{-}H$ absorption bands of guanines, and their possible perturbation by the ligand, which would indicate the onset of hydrogen-bonding interactions in the major groove.

These investigations were carried out on a series of oligonucleotides which encompass the PBS sequence d(GGCGCC)$_2$, its isomer $d(CCCGGG)_2$, and a AT-rich sequence having a $d(CpG)_2$ intercalation site as well as on the polynucleotides poly(dG-dC) and poly(dA-dT) and the salmon sperm DNA. To highlight the role of the arginine side-chains, the complexes of H_2TMPyP-4 were investigated parallel to those of BAP. This investigation has shown some very instructive similarities, as well as differences, between the respective ligand complexes.

UV−visible spectroscopy showed that the binding of BAP to the oligonucleotides, as well as to poly(dG-dC) and salmon sperm DNA, is characterized by substantial hypochromicities and bathochromic shifts of the Soret band of BAP. These are the same spectral signatures observed in the corresponding complexes of H_2TMPyP-4, an indication for intercalating binding. Derivation of the thermal denaturation temperatures from both the 260 nm and the Soret absorption bands showed that the binding of BAP to the oligonucleotides encompassing the PBS sequence resulted in a significant increase of the melting temperature. The most noteworthy shift of 8 °C was obtained with the $d(GGCGCC)_2$ hexamer. Remarkably, the corresponding complexes of BAP with the isomeric sequence $d(CCCGGG)_2$ and the AT-rich one $d(TACGTA)_2$ gave rise to a negligible (1 °C) stabilization. This is a clear indication for the preferential binding of BAP to the PBS-encompassing sequence and is fully consistent with the theoretical predictions. The decisive role of the arginine side-chains into imparting such a selective stabilization is shown by the fact that, in marked contrast to BAP, H_2TMPyP-4 produces a much more modest and identical (3 °C) stabilization of both $d(GGCGCC)_2$ and $d(CCCGGG)_2$. On the other hand, the binding of H_2TMPyP-4 to sequences encompassing the TACGTA hexamer results in a greater (5−10 °C) thermal stabilization, possibly due to additional nonintercalating binding to AT-sites.

The induced-CD and UV−visible results have given evidence to the onset of nonintercalated complexes when the oligonucleotide has an increased content in A−T base pairs. Thus, the binding of BAP and H_2TMPyP-4 to the two GC-rich decamers d(GTGGCGCCAC)$_2$ and d(GTCCCGGGAC)$_2$ yielded a single negative absorption band, characteristic of an intercalation complex. Their binding to the AT-rich decamer d(GTTACGTAAC)$_2$ gave rise to both a positive absorption band, characteristic of nonintercalated binding, and a negative band.

FTIR spectroscopy has shown the complexes of BAP with d(GGCGCC)$_2$ and poly(dG-dC) to be characterized by the presence of a shoulder appearing at 1696 cm^{-1} on the high-frequency side of the C_6═O_6 absorption band of guanine which is located at 1689 cm^{-1}. This high-frequency shift of the C_6═O_6 carbonyl stretching vibration observed upon triplex formation *(92, 93)* was not found in the corresponding complexes of H_2TMPyP-4, an indication for the onset, in the complexes of BAP, of hydrogen bonds involving the arginine side-chains and O_6 of guanine. In addition, FTIR spectroscopy has indicated that, in the complexes of BAP with the GC-rich oligonucleotides as well as with poly(dG-dC), perturbations also occur on the N_7−C_8−H absorption band of guanine, and that they are absent in the corresponding complexes of H_2TMPyP-4. This indication of hydrogen-bonding interactions between N_7 of guanine and the arginine side-chains is conform to our theoretical model. Similar modifications are observed in the FTIR spectra of the complexes of BAP with d(TACGTA)$_2$ indicating interactions with N_7 of adenine, whereas the complexation of H_2TMPyP-4 only affects N_3.

There are very few examples of *de novo* designed intercalating molecules that can bind DNA in the major groove. Two such molecules, mitoxantrone *(102, 103)* and ditercalinium *(86, 87)*, are both endowed with very potent antitumor activities with mitoxantrone used in human chemotherapy. The encouraging results obtained in the present study warrant extensions of this work and an evaluation of the possible therapeutic potency of BAP. Thus, preliminary tests indicate the ability for this molecule to inhibit the early phases of HIV-1 metabolism at concentrations as low as 5×10^{-8} M (Subra et al., private communication).

ACKNOWLEDGMENT

The authors thank the Commissariat à l'Energie Atomique (CEA) and the Département d'Ingénierie des Protéines (Prof. A. Ménez) for giving access to their dichrograph. M.P.-F. gratefully acknowledges Dr. C. Verchère-Béaur (from the Laboratoire de Chimie Bioorganique et Bioinorganique) for helpful comments on UV-visible and circular dichroism results.

REFERENCES

1. Tsimanis, A., Bichko, V., Dreilina, D., Meldrais, J., Lozha, V., Kukaine, R., and Gren, E. (1983) *Nucleic Acids Res. 11,* 6079−6087.
2. Hong, F. D., Huang, H.-J. S., To, H., Young, L.-J. S., Oro, A., Bookstein, R., Lee, E. Y.-H. P., and Lee W.-H. (1989) *Proc. Natl. Acad. Sci. 86,* 5502−5506.
3. Dvorak, M., Urbanek, P., Bartunek, P., Paces, V., Vlach, J., Pecenka, V., Arnold, L., Travnicek, M., and Riman, J. (1989) *Nucleic Acids Res. 17,* 5651−5664.
4. Smith, S., Baker, D., and Jardines, L. (1989) *Biochem. Biophys. Res. Commun. 160,* 1397−1402.
5. Timsit, Y., and Moras, D. (1995) *J. Mol. Biol. 251,* 629−647.
6. Burnouf, D., Koehl, P., and Fuchs, R. P. P. (1989) *Proc. Natl. Acad. Sci. 86,* 4147−4151.
7. Fuchs, R. P. P., Schwartz, N., and Daune, M. P. (1981) *Nature 294,* 657−659.
8. Wain-Hobson, S., Sonigo, P., Danos, O., Cole, S., and Alizon, M. (1985) *Cell 40,* 9−17.
9. Ratner, L., Haseltine, W., Patarca, R., Livak, K. J., Starcich, B., Josephs, S. F., Doran, E. R., Rafalski, J. A., Whitehorn, E. A., Baumeister, K., Ivanoff, L., Petteway, Jr., S. R., Peaerson, M. L., Lautenberger, J. A., Papas, T. S., Ghrayeb, J., Chang, N. T., Gallo, R. C., and Wong-Staal, F. (1985) *Nature 313,* 277−284.
10. Perrée-Fauvet, M., and Gresh, N. (1995) *Tetrahedron Lett. 36,* 4227−4230.
11. Pasternack, R. F., and Gibbs, E. J. (1989) *Metal DNA Chemistry* (Tullius, T., Ed.) pp 59−73, American Chemical Society, Washington, DC.
12. Pasternack, R. F., and Gibbs, E. J. (1996) *Metal Ions in Biological Systems* (Sigel, A., and Sigel, H., Ed.) *33,* pp 367−397, Marcel Dekker Inc., New York.
13. Fiel, R. J., Howard, J. C., Mark, E. H., and Datta Gupta, N. (1979) *Nucleic Acids Res. 6,* 3093−3118.
14. Ornstein, R., and Rein, R. (1979) *Biopolymers 18,* 2821−2847.
15. Miller, K., and Picior, J. (1979) *Biopolymers 18,* 2683−2719.
16. Pack, G., and Loew, G. H. (1979) *Biochim. Biophys. Acta 519,* 163−172.
17. Nuss, M., Marsh, F., and Kollman, P. A. (1979) *J. Am. Chem. Soc. 101,* 825−833.
18. Villanueva, A., Caggiari, L., Jori, G., and Milanesi, C. (1994) *J. Photochem. Photobiol. B: Biol. 23,* 49−56.
19. Villanueva, A., Juarranz, A., Diaz, V., Gomez, J., and Canete, M. (1992) *Anti-Cancer Drug Des. 7,* 297−303.
20. Praseuth, D., Gaudemer, A., Verlhac, J. B., Kraljic, I., Sissoëff, I., and Guillé, E. (1986) *Photochem. Photobiol. 44,* 717−724.
21. Byrnes, R. W., Fiel, R. J., and Datta-Gupta, N. (1988) *Chem.-Biol. Interact. 67,* 225−241.
22. Bernardou, J., Pratviel, G., Bennis, F., Girardet, M., and Meunier, B. (1989) *Biochemistry 28,* 7268−7275.
23. Dabrowiak, J. C., Ward, B., and Goodisman, J. (1989) *Biochemistry 28,* 3314−3322.
24. Van Atta, R. B., Bernardou, J., Meunier, B., and Hecht, S. M. (1990) *Biochemistry 29,* 4783−4789.
25. Pratviel, G., Duarte, V., Bernardou, J., and Meunier, B. (1993) *J. Am. Chem. Soc. 115,* 7939−7943.
26. Seeman, N., Rosenberg, J., and Rich, A. (1976) *Proc. Natl. Acad. Sci. 73,* 804−808.
27. Hélène, C. (1977) *FEBS. Lett. 74,* 10−14.
28. Desjarlais, J. R., and Berg, J. M. (1992) *Proteins: Structure, Functions, and Genetics 12,* 101−104.
29. Desjarlais, J. R., and Berg, J. M. (1992) *Proc. Natl. Acad. Sci. 89,* 7345−7349.
30. Choo, Y., and Klug, A. (1994) *Proc. Natl. Acad. Sci. 91,* 11163−11167, 11168−11172.
31. Jamieson, A. C., Kim, S.-H., and Wells, J. A. (1994) *Biochemistry 33,* 5689−5695.
32. Lustig, M., and Jernigan, R. L. (1995) *Nucleic Acids Res. 23,* 4707−4711.
33. Rebar, E. J., and Pabo, C. O. (1994) *Science 263,* 671−673.
34. Suzuki, M., Gerstein, M., and Yagi, N. (1994) *Nucleic Acids Res. 22,* 3397−3405.
35. Wu, H., Yang, W. R., and Barbas III, C. F. (1995) *Proc. Natl. Acad. Sci. 92,* 344−348.
36. Pavletich, N. P., and Pabo, C. O. (1991) *Science 252,* 809−817.
37. Pavletich, N. P., and Pabo, C. O. (1993) *Science 261,* 1701−1707.
38. Marmorstein, R., Carey, M., Ptashne, M., and Harrison, S. C. (1992) *Nature 356,* 408−414.
39. Konig, P., Giraldo, R. Chapman, L., and Rhodes, D. (1996) *Cell 85,* 125−136.

40. Baleja, J. D., Marmorstein, R., Harrison, S. C., and Wagner, G. (1992) *Nature 356*, 450−453.
41. Gresh, N., and Kahn, P. H. (1990) *J. Biomol. Struct. Dynam. 7*, 1141−1160.
42. Gresh, N., and Kahn, P. H. (1991) *J. Biomol. Struct. Dynam. 8*, 827−846.
43. Gresh, N., René, B., Hui, X., Barsi, M.-C., Roques, B. P., and Garbay, C. (1994) *J. Biomol. Struct. Dynam. 12*, 91−110.
44. Gresh, N. (1996) *J. Biomol. Struct. Dynam. 14*, 255−273.
45. Terbrueggen, R. H., and Barton, J. K. (1995) *Biochemistry 34*, 8227−8234.
46. Tabor, A. B. (1996) *Tetrahedron 52*, 2229−2234.
47. Morii, T., Saimei, Y., Okagami, M., Makino, K., and Sugiura, Y. (1997) *Biochemistry 119*, 3649−3655.
48. Cuenoud, B., and Scheparz, A. (1993) *Science 259*, 510−513.
49. Park, C., Campbell, J. L., and Goddard, III, W. A. (1995) *J. Am. Chem. Soc. 117*, 6287−6291.
50. Moser, H. E., and Dervan, P. B. (1987) *Science 238*, 645−650.
51. Le Doan, T., Perrouault, L., Praseuth, D., Habhoub, N., Decout, J.-L., Thuong, N. T., Lhomme, J., and Hélène, C. (1987) *Nucleic Acids Res. 15*, 7749−7760.
52. Hélène, C., and Toulmé, J. J. (1990) *Biochim. Biophys. Acta 1049*, 99−125.
53. De Mesmaeker, A., Häner, R., Martin, P., and Moser H. E. (1995) *Acc. Chem. Res. 28*, 366−374.
54. Escudé, C., Nguyen, C. H., Mergny, J. L., Sun, J. S., Bisagni, E., Garestier T., and Hélène, C. (1995) *J. Am. Chem. Soc. 117*, 10212−10219.
55. Hyrup, B., and Nielsen P. E. (1996) *Bioorg. Med. Chem. 4*, 5−23.
56. Luo, J., and Bruice, T. C. (1997) *J. Am. Chem. Soc. 119*, 6693−6701.
57. Arcamone, F. (1981) *Doxorubicin, Anticancer Antibiotics.* Academic Press, New York.
58. Lee, S. H., and Goldberg, I. H. (1989) *Biochemistry 28*, 1019−1026.
59. Zein, N., Poncin, M., Nilakantna, R., and Ellestad, G. A. (1989) *Science 244*, 697−699.
60. Ho, S. N., Boyer, S. H., Schreiber, S. L., Danishefshky, S. J., and Crabtree, G. R. (1994) *Proc. Natl. Acad. Sci. 91*, 9203−9207.
61. Zimmer, C., and Wahnert, U. (1986) *Progress Biophys. Mol. Biol. 41*, 31−112.
62. Mrksich, M., Wade, W. S., Dwyer, T. J., Geierstanger, B. H., Wemmer, D. E., and Dervan, P. B. (1992) *Proc. Natl. Acad. Sci. 89*, 7586−7590.
63. Dwyer, T. J., Geierstanger, B. H., Bathini, Y., Lown, J. W., and Wemmer, D. E. (1992) *J. Am. Chem. Soc. 114*, 5911−5919.
64. Nikolaev, V. A., Grokhovsky, S. L., Surovaya, A. N., and Gursky, G. V. (1996) *J. Biomol. Struct. Dynam. 14*, 31−47.
65. Bailly, C., Helbecque, N., Hénichart, J.-P., Colson, P., Houssier, C., Rao, K. E., Shea, R. G., and Lown, J. W. (1990) *J. Mol. Recognit. 3*, 26−35.
66. Bailly, C., and Hénichart, J.-P. (1991) *Bioconjugate Chem. 2*, 379−393.
67. Anneheim-Herbelin, G., Perrée-Fauvet, M., Gaudemer, A., Hélissey, P., Giorgi-Renault, S., and Gresh, N. (1993) *Tetrahedron. Lett. 34*, 7263−7266.
68. Goulaouic, H., Carteau, S., Subra, F., Mouscadet, J.-F., Auclair, C., and Sun, J.-S. (1994) *Biochemistry 33*, 1412−1418.
69. Bourdouxhe-Housiaux, C., Colson, P Houssier, C., Waring, M. J., and Bailly, C. (1996) *Biochemistry 35*, 4251−4264.
70. Hélissey, P., Bailly, C., Vishwakarma, J. N., Auclair, C., Waring, M. J., and Giorgi-Renault, S. (1996) *Anti-Cancer Drug Des. 11*, 527−551.
71. Steitz, T. A. (1990) *Quart. Rev. Biophys. 23*, 205−280.
72. Pasternack, R. F., Gibbs, E. J., and Villafranca, J. J. (1983) *Biochemistry 22*, 2406−2414.
73. Pasternack, R. F.; Huber, P. R., Boyd, P., Engasser, G., Francesconi, L., Gibbs, E., Fasella, P., Cerio Venturo, G., and Hinds, L. deC. (1972) *J. Am. Chem. Soc. 94*, 4511−4517.
74. Cantor, C. R. and Warshaw, M. M. (1970) *Biopolymers 9*, 1059−1077.
75. Hui, X., and Gresh, N. (1993) *J. Biomol. Struct. Dynam. 11*, 333−334.
76. Perrée-Fauvet, M., and Gresh, N. (1994) *J. Biomol. Struct. Dynam. 11*, 1203−1224.
77. Lavery, R. (1988) in *Unusual DNA Structures* (Wells, R. D., and Harvey, S. C., Eds.), 189−206, Springer-Verlag, New York.
78. Lavery, R. (1994) *Adv. Comput. Biol. 1*, 69−145.
79. Pullman, B., and Pullman, A. (1981) *Quart. Rev. Biophys. 14*, 289−380.
80. Carvlin, M. J. and Fiel, R. J. (1983) *Nucleic Acids Res. 11*, 6121−6139.
81. Carvlin, M. J., Mark, E., Fiel, R. J. and Howard, J. C. (1983) *Nucleic Acids Res. 11*, 6141−6154.
82. Kelly, J. M. and Murphy, M. (1985) *Nucleic Acids Res. 13*, 166−184.
83. Sehlstedt, U., Kim, S. K., Carter, P., Goodisman, J., Vollano, J. F., Nordén, B. and Dabrowiak, J. C. (1994) *Biochemistry 33*, 417−426.
84. Hui, X., Gresh, N., and Pullman, B. (1990) *Nucleic Acids Res. 18*, 1109−1114.
85. Rentzeperis, D., and Marky, L. A. (1993) *J. Am. Chem. Soc. 115*, 1645−1650.
86. Garbay-Jaureguiberry, C., Esnault C., Delepierre M., Laugaa P., Laalami, S., Le Pecq, J.-B., and Roques, B. P. (1987) *Drugs Exptl. Clin. Res. XIII*, 353−357.
87. Garbay-Jaureguiberry, C., Barsi, M.-C., Jacquemin-Sablon, A., Le Pecq, J.-B., and Roques, B. P. (1992) *J. Med. Chem. 35*, 72−81.
88. Pasternack, R. F., Brigandi, R. A., Abrams, M. J. and Gibbs, E. J. (1990) *Inorg. Chem. 29*, 4483−4486.
89. Bustamante C., Gurrieri, S., Pasternack, R. F., Purrello, R. and Rizzarelli, E. (1994) *Biopolymers 34*, 1099−1104.
90. Tsuboi, M., Takahashi, S. and Harda, I. (1973) In *Physicochemical properties of Nucleic Acid.* Duchesne, G. (Ed.) Academic Press, London, Vol. 2, pp 91−145.
91. Tsuboi, M. (1974) *In Basic Principles in Nucleic Acid Chemistry*, Paul, O. P. Ts'o. (Ed.) Academic Press, London. Vol. 1, pp 399−452.
92. Akhebat, A., Dagneaux, C., Liquier, J. and Taillandier, E. (1992) *J. Biomol. Struct. Dynam. 10*, 577−588.
93. Ouali, M., Letellier, R., Sun, J. S., Akhebat, A., Adnet, F., Liquier, J. and Taillandier, E. (1993) *J. Am. Chem. Soc. 115*, 4264−4270.
94. Taboury, J. A., Bourtayre, P., Liquier, J. and Taillandier, E. (1984) *Nucleic Acids Res. 12*, 4247−4258.
95. Majoube, M. (1984) *J. Chim. Phys. 81*, 303−315.
96. Ghomi, M. and Taillandier, E. (1985) *J. Biophys. 12*, 153−162.
97. Adam, S., Bourtayre, P., Liquier, J. and Taillandier, E. (1986) *Nucleic Acids Res. 1*, 3501−3513.
98. Benevides, J. M. and Thomas, G. J. Jr. (1985) *Biopolymers 24*, 667−682.
99. Liquier, J., Mchami, A.; Taillandier E. (1989) *J. Biomol. Struct. Dynam. 7*, 119−126.
100. Strangret, J., and Savoie, R. (1992), *Can. J. Chem. 70*, 2875−2882.
101. Nonaka, Y., Lu, D. S., Dwivedi, A., Strommen, D. P. and Nakamoto, K. (1990) *Biopolymers 29*, 999−1004.
102. Murdock, K. C., Child, R. C., Fabio, P. F., Angier, R. B., Wallace, R. E., Durr, F. E., and Citarella, R. V. (1979) *J. Med. Chem. 22*, 1024−1030.
103. Wallace, R. E., Murdock, K. C., Angier, R. B., and Durr, F. E. (1979) *Cancer Res. 39*, 1570−1574.

BI972964H